JFBE 6(1): 1-7, 2023

Journal of Food and Bioprocess Engineering

Journal homepage: https://jfabe.ut.ac.ir

Original research

# Fabrication and physicochemical characterization of electrospun nanofibers using Chia seed mucilage

Samira Dehghani[a]; Mohammad Noshad[a,*]; Saadat Rastegarzadeh[b]; Mohammad Hojjati[a]; Ali Fazlara[c]

[a] *Department of Food Science & Technology, Agricultural Sciences & Natural Resources University of Khuzestan, Mollasani, Iran*
[b] *Department of Chemistry, Faculty of Science, Shahid Chamran University of Ahvaz, Ahvaz, Iran*
[b] *Department of Food Hygiene, Faculty of Veterinary Medicine, Shahid Chamran University of Ahvaz, Ahvaz, Iran*

A B S T R A C T

In this study, Chia seed mucilage (CSM) as a new source and polyvinly alcohol (PVA) as co-polymer was used to prepare of nanofibers. Different solutions with CSM/PVA volume ratios of 100:0, 80:20, 60:40, 40:60, 20:80, 0:100 were prepared. Results show the increase in the CSM in the polymer solution increased the viscosity, electrical conductivity and viscosity of solution. Scanning electron microscopy (SEM) was to evaluate the morphology of nanofibers. Fourier transform infrared spectrometer (FTIR), X-ray diffraction (XRD), and thermogravimetric analysis (TGA) studies were used to evaluate chemical structure, crystalline structure and thermal characteristics of nanofibers of CSM/PVA. The crystallization index of CSM, PVA, and CSM/PVA nanofibers was 52%, 38%, and 44%, respectively. The non-formation of a new peak and presence of CSM and PVA peaks in the FTIR spectrum of the produced nanofibers are indicative of the lack of chemical reactions between CSM and PVA. Also, the addition of PVA to CSM improves the thermal resistance of the nanofibers.

Keywords: Chia seed mucilage; FTIR; XRD; TGA

Received 17 May 2022; Revised 15 July 2022; Accepted 15 July 2022



## 1. Introduction

Nanotechnology has attracted attention in the food industry due to its ability to create compounds with novel properties (He et al., 2019). In this regard, the production of nanofibers has also garnered undivided attention in recent years. Nanofibers are extremely thin threads with a large length to diameter ratio (L/D), which increases their functions. Among the nanofiber production methods, electrospinning is the most efficient method for producing different types of nanofibers from polymer solutions due to its high surface area to volume ratio, high porosity, and production in the noncontact mode. In electrospinning, nanofibers are produced through the application of high electrical voltage to the polymer solution and evaporation of the contained solvent (Zhang et al., 2020; Leidy & Ximena, 2019). Therefore, electrospinning can be used to convert different types of natural biopolymers such as proteins and polysaccharides into fibers on the nanoscale (Kumar et al., 2019).

Mucilage is one of the most important types of hydrocolloids that are abundantly available in nature (Urena-Saborio et al., 2018). Today, mucilage is used as a new source of biopolymers in the production of nanofibers (Kurd et al., 2017; Hadad & Goli 2018; Golkar et al., 2019; Allafchian et al., 2019; Sen et al., 2022). Besides, chia seed mucilage is used as a new source of hydrocolloids in the food industry due to its biocompatibility and biodegradability (Fernandes & de las Mercedes Salas-Mellado 2017; de Campo et al., 2017). Chia seed, with the scientific name of *Salvia hispanica* L., contains 5% mucilage and it is commercially cultivated and marketed in the Americas. Chia seed mucilage is a branched polysaccharide, which is composed of xylose, mannose, arabinose, glucose, galacturonic acid, and glucuronic acid. Chia seed mucilage is highly water soluble and forms a highly viscos solution with low concentrations (Goh et al., 2016; de Campo et al., 2017).

Polyvinyl alcohol (PVA) with hydrocarbon backbone is a water-soluble, nontoxic, and biodegradable synthetic polymer. It can form a bond with other polymers and it is used in electrospinning with other hydrocolloids (Yang et al., 2016; Adeli

*Corresponding author.
E-mail address: noshad@asnrukh.ac.ir (M. Noshad).
https://doi.org/10.22059/jfabe.2022.343218.1114

et al., 2019). Fahami and Fathi (2018) studied the production of nanofibers from cress seed mucilage using PVA. They produced cress seed mucilage nanofibers (3%) and PVA (10%) with different ratios (80:20, 60:40, 40:60, 20:80). They reported that cress mucilage nanofibers/PVA with a ratio of 40:60 and a mean diameter of 172.2 ± 43.5 nm were selected as the best sample (Fahami & Fathi, 2018b). Moreover, Sousa et al. (2015) used 10% PVA solution as a co-spinning agent in combination with 1% agar gum with 0:100, 50:50, 70:30, 80:20, and 100:0 ratios. The results of this study indicated that the 70:30 ratio of agar gum to PVA is the optimal ratio for the production of nanofibers (Sousa et al., 2015).

Since the production of nanofibers from chia seed mucilage has not been carried out, the production and physicochemical properties of chia seed mucilage (CSM) and PVA nanofibers were evaluated in this study.

## 2. Material and Methods

### 2.1. Materials

Argentinean chia seed was purchased from the local farmer's market in Khuzestan province of Iran. For the analytical test, chemicals such as PVA (Mw: 145000 g/mol), Hydrochloric acid, acetic acid, ethanol and 2,2-Diphenyl-1-picrylhydrazyl were purchased from Merck, Darmstadt, Germany.

### 2.2. Chia seed mucilage extraction

For extraction of mucilage, distilled water was added to chia seed (25 to 1 (w/w)). After, 30 min, the extracted mucilage was separated by extruder. The obtained mucilage was centrifuged (Hermle, Z206A, Germany) and then dried for 48 h by freeze dryer (SBPE, SUT-01, Iran) (Noshad et al., 2019).

### 2.3. Preparation of solutions

To prepare the solution, first, the powder of dried Chia seed mucilage (CSM) was added to the mixture of deionized water/acetone (7:3, v/v). Then, by adding 10.0 g polyvinyl alcohol powder to deionized water (80 ºC) was prepared 100 ml solution of PVA. To full hydration, the obtained solutions were held in the refrigerator for 24 h. Finally, different solutions with CSM/PVA volume ratios of 100:0, 80:20, 60:40, 40:60, 20:80, 0:100 were prepared.

### 2.4. Viscosity of the electrospinning solutions

The Brookfield DV-II+Pro Viscometer was used to access the viscosity of CSM, PVA and CSM/PVA volume ratios (100:0, 80:20, 60:40, 40:60, 20:80, 0:100) solutions (Kurd et al., 2017).

### 2.5. Electrical conductivity of electrospinning solutions

Digital electro conductivity meter (Jenway, 4510, England) was used to measure the electrical conductivity of CSM, PVA and CSM/PVA volume ratios (100:0, 80:20, 60:40, 40:60, 20:80, 0:100) solutions (Fahami & Fathi, 2018a).

### 2.6. Electrospinning conditions

The electrospinning device (eSpinner NF C-AN/VI, Iran) with high voltage power (18 and 23 kV), distance between needle tip and collector (12 cm), and a feed rate of 0.4 ml/h were used to electrospin of CSM/PVA solution with different concentrations.

### 2.7. Scanning electron microscopy

Scanning electron microscopy (SEM) (LEO 1455 VP) was used to investigate the nanofiber morphology. For improve conductivity during imaging, the samples were covered with 5-6 nm thickness of gold (Kurd et al., 2017).

### 2.8. X-ray diffraction

A Philips X'Pert diffractometer was used with a radiation of Cu Kα (λ-1.54 Å), 40kV voltage, and 2θ = 10-100 to analyze the X-Ray diffraction patterns (XRD) of CSM. PVA and CSM/PVA nanofibers (Londhe et al., 2019).

### 2.9. Fourier transform infrared (FTIR)

The chemical structures of CSM/PVA nanofibers (with CSM/PVA volume ratios (100:0, 80:20, 60:40, 40:60, 20:80, 0:100) were evaluated in the region 4000-400 $cm^{-1}$ by Fourier transform infrared spectroscopy (Model 1725X, Perkin Elmer, Norwalk, CT, USA) (Ellerbrock et al., 2019).

### 2.10. Thermal gravimetric analysis (TGA)

The Simultaneous Thermal Analyzer (STA) (STA 504, Bahr, Germany) was used to evaluate thermal analysis (TG-DTA) of CSM, PVA, CSM/PVA nanofibers at a temperature range of 50 to 300 °C, heated rate of 10 °C/min under the argon atmospheric condition (Kéri et al., 2019).

### 2.11. Statistical Analysis

The experiments were conducted as factorial arrangement in the completely randomized design. Duncan's multiple range test was performed to test the statistical significance of the data and ANOVA (analysis of variance) was used to analyze the results with SPSS 16.

## 3. Results and Discussion

### 3.1. Viscosity

One of the most important factors influencing the production of nanofibers is the viscosity of the polymer solution. A solution with low viscosity results in the formation of spindle-like beads instead of nanofibers. As viscosity reaches the critical viscosity level, the formation of spindle-like beads decreases and nanofibers start to form. The spindle-like beads re-emerge with an increase in viscosity from the critical viscosity, which could be attributed to the current thrown by the tip of the needle at the collector. Since the molecular weight of the polymers and the concentration of the polymer solution affect the viscosity of the polymer solution, the

optimal viscosity of each polymer solution has to be determined (Okutan et al., 2014; Kurd et al., 2017). Table 1 shows the effect of the polymer solution viscosity on the morphology of the nanofibers. According to the results (Table 1), the increase in the CSM in the polymer solution increased the polymer solution viscosity, which could be attributed to the higher molecular weight of CSM as compared to PVA (Fahami & Fathi, 2018a). The results reported by Kurd et al. (2017), also showed that the increase in PVA to basil mucilage ratio reduced the viscosity of the polymer solution. They attributed this trend to the variation or destruction of the intramolecular and intermolecular bonds of the basil seed mucilage threads (Kurd et al., 2017).

Table 1. Effect of different rations concentration of CSM/PVA on viscosity and electrical conductivity of biopolymer solutions.

| The ratios of CSM/PVA concentration | Viscosity (cP) | Conductivity (µS/cm) |
|---|---|---|
| 100:0 | 1297.82 ± 8.74[a] | 1805 ± 75[a] |
| 80:20 | 1099.5 ± 5.9[b] | 1543.5 ± 32.5[b] |
| 60:40 | 1044.3 ± 10.7[c] | 1437 ± 37[c] |
| 40:60 | 980.4 ± 9.1[d] | 1361.5 ± 3.5[d] |
| 20:80 | 895.7 ± 10.7[e] | 1251.5 ± 23.5[e] |
| 0:100 | 756.3 ± 7.4[f] | 733.5 ± 22.5[f] |

Columns with different letters differ statistically ($p < 0.05$).

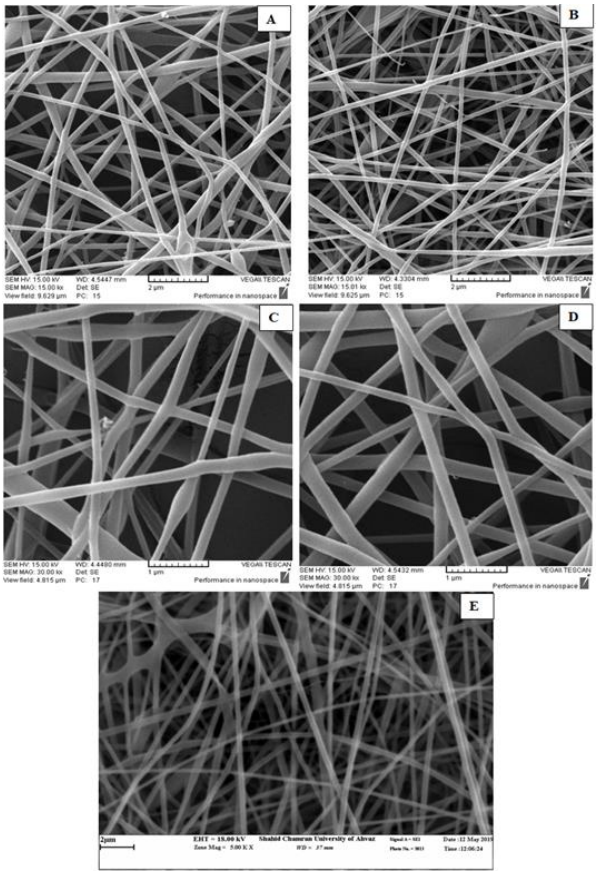


Fig. 1. Effect of different rations concentration of CSM/PVA on morphology of nanofibers. A: CSM to PVA volume ratios = 0:100; B: 20:80; C = 40:60; D = 60:40; E = 80:20.

## 3.2. *Electrical conductivity*

Table 1 shows the results of measuring the electrical conductivity of different solutions. According to the results Table 1, the electrical conductivity of the solutions decreased as the level of PVA increased. This could be attributed to the lower electrical conductivity of PVA (733.5 ± 22.5 µs/cm) as compared to CSM (1805 ± 75 µs/cm). The low electrical conductivity of the solution led to the formation of spindle-like beads and non-uniform nanofibers, which was probably caused by the inadequate tension in the resulting nanofibers in the electric field (Gu et al., 2005; Hamrang & Howell, 2013; Haghi & Akbari, 2007).

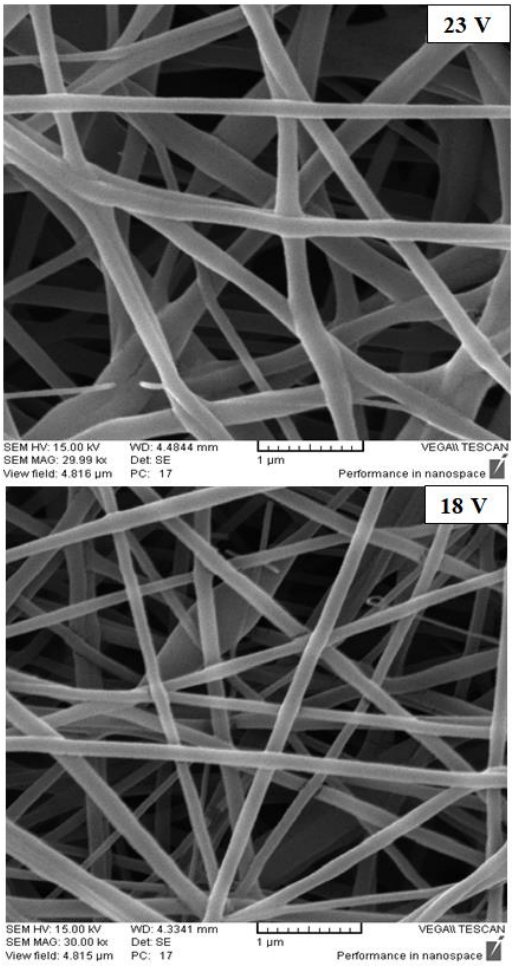


Fig. 2. Effect of different voltage of the electrospinning device on morphology of nanofibers (CSM/PVA ratios = 60:40).

## 3.3. *Morphology of nanofibers*

A scanning electron microscope was used to analyze the morphology of the nanofibers. Our morphological analysis of the nanofibers indicated that the increase in CSM in the polymer solution reduced the diameter of the nanofibers (Fig. 1). It was probably caused by the presence of anionic groups (hydroxyl and carboxyl groups) in the structure of CSM, which improved the

electrical conductivity of the polymer solution, load distribution, and the polymer jet during electrospinning. As a result, more tensile forces are exerted to the nanofibers, reducing the diameter of nanofibers (Golkar et al., 2019; Kurd et al., 2017). The results of this study were agreed with the results reported by Fahami and Fathi (2018). The results of this study showed that the increase in the concentration of cress seed mucilage in the polymer solution reduced the diameter of nanofibers during electrospinning (Fahami & Fathi, 2018a).

Moreover, the results showed that the increase in the voltage of the electrospinning device from 18 to 23kV increased the diameter of nanofibers, leading to the production of smooth nanofibers without spindle-like beads (Fig. 2). To explain this trend, it could be stated that the increase in the voltage of the electrospinning device increased the electric field, which led to the outflow of more polymer solution from the needle tip in the electrospinning device. The increased outflow of the polymer solution prevented the rapid evaporation and elongation of the nanofibers, thereby increasing the diameter of the produced nanofibers (Şener et al., 2011; Motamedi et al., 2017). The results of this study complied with the findings reported by (Liu et al., 2011; Fahami & Fathi, 2018b; Hadad & Goli, 2018).

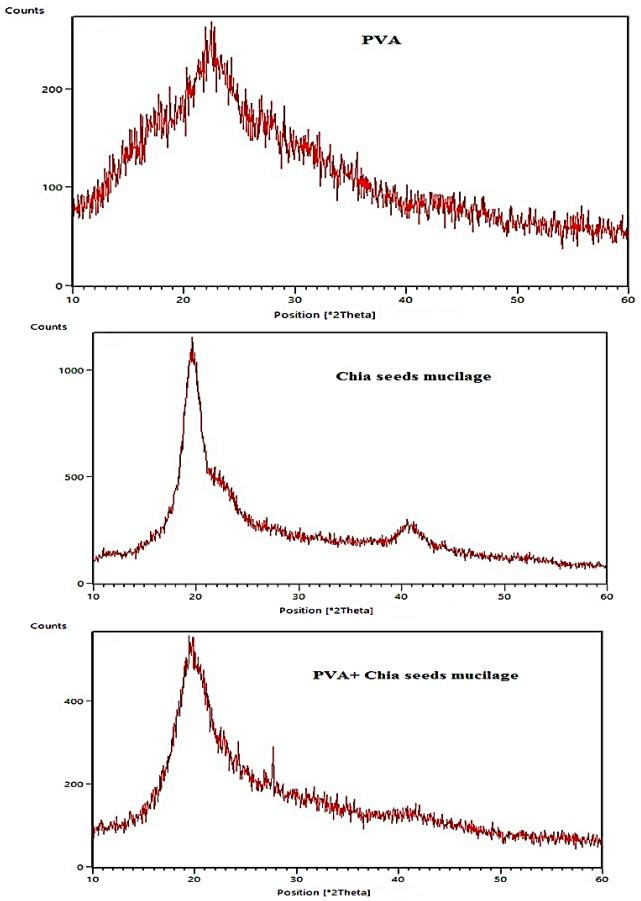


Fig. 3. XRD patterns of CSM (A), PVA (B) and CSM/PVA nanofibers (CSM/PVA ratios = 60:40) (C).

Based on the scanning electron microscope (SEM) images, the 40:60 ratios of CSM/PVA, and an electrospinning voltage of 18kV were selected as the optimal condition for the production of nanofibers. Thereafter, infrared spectroscopy (IR spectroscopy), X-ray diffraction, and thermogravimetric analysis tests were conducted on the nanofibers produced in this condition.

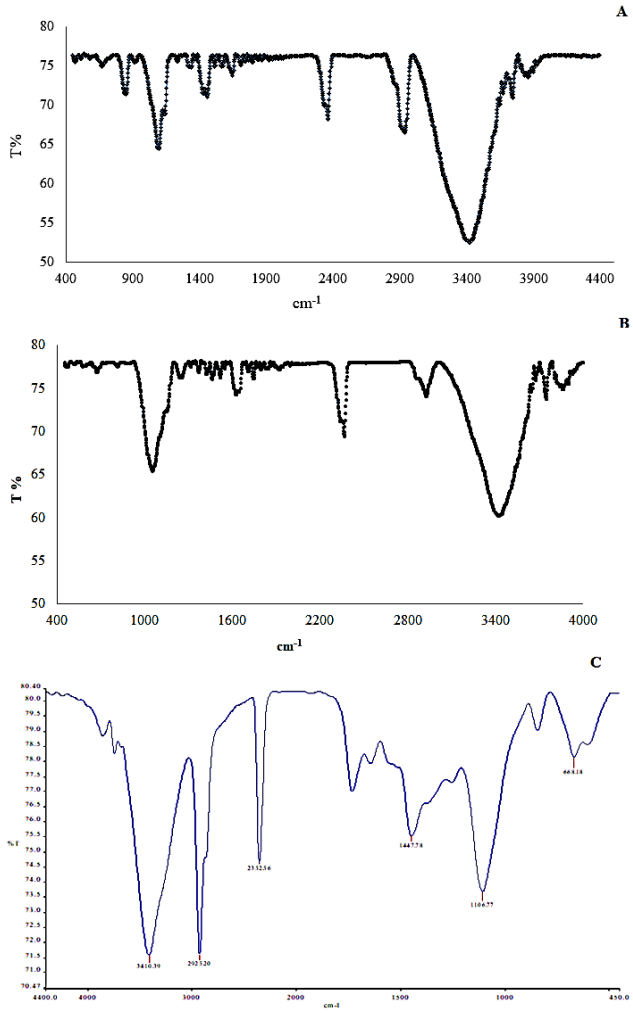


Fig. 4. FTIR of CSM (A), PVA (B) and CSM/PVA nanofibers (CSM/PVA ratios = 60:40) (C).

### 3.4. *X-ray diffraction*

X-ray diffraction is used to analyze and determine the crystalline structure and amorphous crystals. The crystalline pattern of CSM, PVA, and CSM/PVA nanofibers is depicted in Fig. 3. As seen (Fig. 3A), the presence of two diffraction peaks at 2θ =20 and 2θ = 41 is indicative of the crystalline structure of CSM. The presence of a wide peak (2θ = 21.5) in the PVA spectrum also shows the existence of a semi-crystalline structure (Fig. 3B). The presence of the peak in region 2θ = 20 in the XRD of CSM/PVA nanofibers is linked to the CSM peak (Fig. 3C).

ARIAN Pro software is used to determine the crystallization index of the samples. For this purpose, the x and y data resulting from the software X-Ray diffraction (XPert HighScore Plus, 3.0.5) is also used. Eq. 1 calculates the crystallization index:

$$Crystallization\ index = \frac{Crystalline\ region\ surface\ area}{Total\ surface\ area} \quad (1)$$

The crystallization index of CSM, PVA, and CSM/PVA nanofibers was 52%, 38%, and 44%, respectively. In a study by Kurd et al. (2017), the crystalline pattern of basil mucilage/PVA nanofibers was analyzed. Based on the results of this study, the crystallization index of basil mucilage, PVA, and basil mucilage/PVA nanofibers was 54%, 35%, and 43%, respectively.

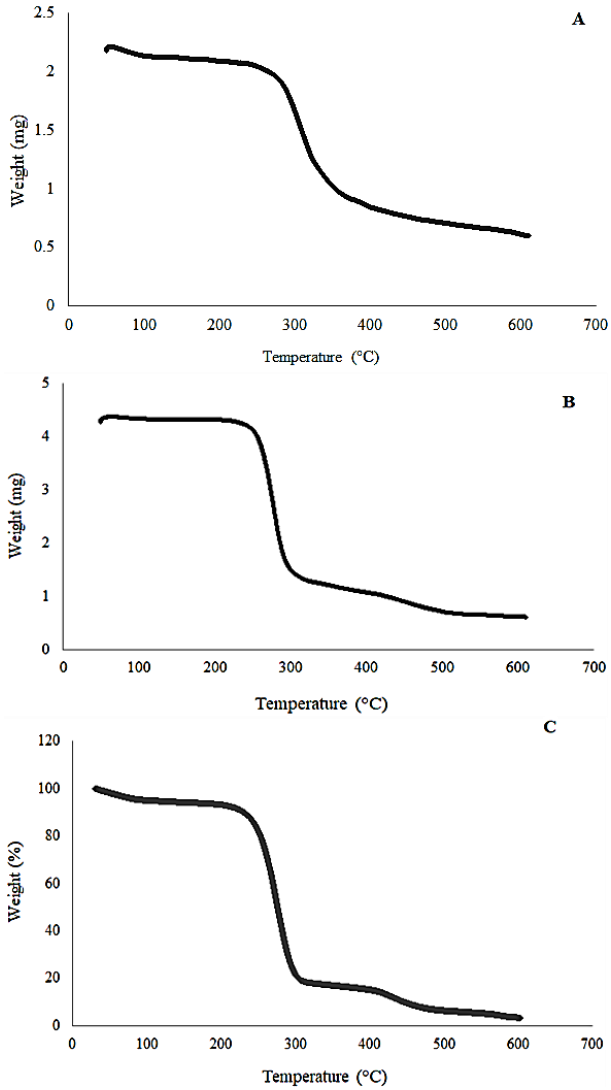


Fig. 5. Thermogravimetric analysis of CSM (A); PVA (B) and CSM/PVA nanofibers (CSM/PVA ratios = 60:40) (C).

### 3.5. *Fourier-transform infrared (FTIR) spectroscopy*

A FTIR spectroscopy analysis was carried out to study the chemical structure of CSM and PVA, and the possible interactions between CSM and PVA in the produced nanofibers.

The following figures show the FTIR spectrum of CSM, PVA and CSM/PVA nanofibers (Fig. 4). The FTIR spectrum of CSM can be classified into 5 categories: 1) 3200-3600 $cm^{-1}$, 2) 3000-2800 $cm^{-1}$, 3) 2600-2000 $cm^{-1}$, 4) 1600-1500 cm-1, and 5) 1300-1000 $cm^{-1}$ (Fig. 4A). The 3200-3600 $cm^{-1}$ resulted from the hydroxyl (OH) groups. The presence of peaks in the 2800-3000 $cm^{-1}$, which was the characteristic of the tension in the C-H bonds of the methyl groups and the presence of a peak in the 2000-2600 $cm^{-1}$ (with 2348 $cm^{-1}$ as the center) reflected the presence of the C=O tensile bond (carbonyl) in the sample. Besides, the presence of peaks in the 1500-1600 $cm^{-1}$ showed the presence of the C=O tensile bond (carboxyl group), which could be attributed to the presence of uronic acid in the sample structure. The peak in 1146 $cm^{-1}$ can also be attributed to the presence of C-O-C tensile groups in the structure (Ellerbrock et al., 2019; Darwish et al., 2018).

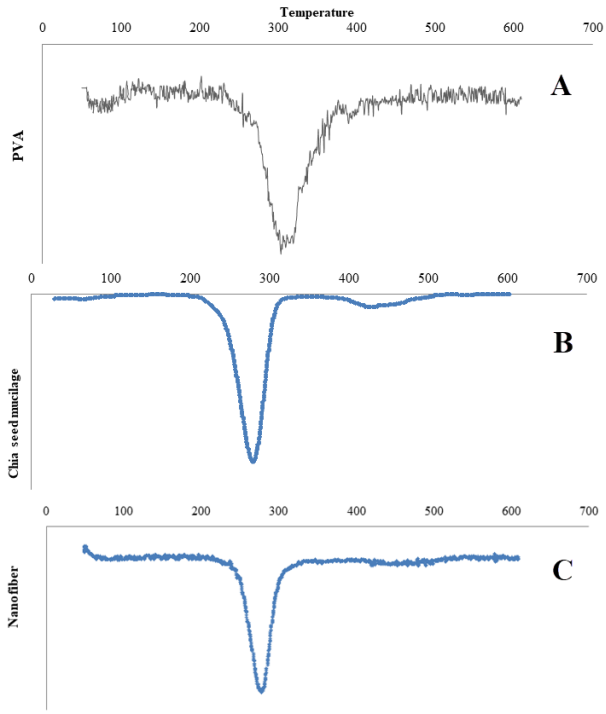


Fig. 6. First derivatives of TGA results for CSM (A), PVA (B) and CSM/PVA nanofibers (CSM/PVA ratios = 60:40) (C).

The FTIR spectrum of PVA shows the presence of the hydroxyl group (peak in the 3450 $cm^{-1}$), the –CH2 group (peak in the 2900 $cm^{-1}$), the C=O group associated with non-hydrolyzed acetate (peak in the 1740 $cm^{-1}$), CH-O-H group (peak in the 1420 $cm^{-1}$), C-O group (peak in the 1100 $cm^{-1}$), and C-C group (peak in the 850 $cm^{-1}$) in its structure (Fig. 4B) (Alhosseini et al., 2012).

The non-formation of a new peak and presence of CSM and PVA peaks in the FTIR spectrum of the produced nanofibers are indicative of the lack of chemical reactions between CSM and PVA (Fig. 4C).

### *3.6. TGA*

The thermogravimetric analysis technique can be used to study the thermogravimetric stability of biopolymers (Menczel & Prime, 2009). Fig. 5A shows the variations of weight with temperature for CSM. Based on Fig. 5A, in three thermal ranges, the weight of CSM: 1) the ambient temperature to 115 ℃ temperature, which is associated with the evaporation of water in samples; 2) the 190 to 330 ℃, which is linked to the breakdown and destruction of the biopolymers; 3) the 340 to 6000 ℃, which probably due to the continued breakdown and destruction of the biopolymers (Kurd et al., 2017; Fahami & Fathi, 2018b).

The variations of weight with temperature are depicted in Fig. 5B for PVA. As seen, the highest decrease in weight was observed in the 270-490 ℃, which could be attributed to the breakdown and destruction of the main branches and sub-branches of PVA (Fahami & Fathi, 2018b).

The variations of weight with temperature for CSM/PVA nanofibers are depicted in Fig. 5C. As seen (Fig. 5C), the first decrease in weight was observed in the ambient temperature to 110 ℃, which was probably caused by the evaporation of water and the solvent in the samples. Moreover, the highest decrease was observed in the 190-460 ℃, which was linked to the breakdown and destruction of the biopolymers (Kayaci et al., 2013).

The first derivative thermogravimetric curve can be used to determine the temperature at which the biopolymer shows the highest level of thermal stability. The first derivative thermogravimetric curve of CSM, PVA, and CSM/PVA nanofibers is depicted in Fig. 6. According to the results (Fig. 6), at the 280 ℃ and 310 ℃ temperatures, CSM and PVA show the highest levels of thermal stability, respectively. Moreover, the addition of PVA to CSM improves the thermal resistance of the nanofibers (Camelo Caballero et al., 2019)

## 4. Conclusion

In this study, electrospinning process was used to produce nanofibers of CSM/PVA. Results showed incorporating PVA in CSM nanofibers reduced of electrical conductivity and viscosity of biopolymer solution. Based on the scanning electron microscope (SEM) images, the 40:60 ratios of CSM/PVA, and an electrospinning voltage of 18kV were selected as the optimal condition for the production of nanofibers. FTIR confirmed no chemical reactions between CSM and PVA in the nanofibers. According to the results, at the 280 ℃ and 310 ℃ temperatures, CSM and PVA show the highest levels of thermal stability, respectively. Moreover, the addition of PVA to CSM improves the thermal stability of the nanofibers.

## Acknowledgment

The authors wish to express their profound gratitude sincerely to the Research Deputy of Agricultural Sciences and Natural Resources University of Khuzestan for financially supported this project.

## Conflict of interest

The authors declared that they have no conflict of interest.

## References

Adeli, H., Khorasani, M. T., & Parvazinia, M. (2019). Wound dressing based on electrospun PVA/chitosan/starch nanofibrous mats: Fabrication, antibacterial and cytocompatibility evaluation and in vitro healing assay. *International Journal of Biological Macromolecules*, *122*, 238-254.

Alhosseini, S. N., Moztarzadeh, F., Mozafari, M., Asgari, S., Dodel, M., Samadikuchaksaraei, A., Kargozar, S., & Jalali, N. (2012). Synthesis and characterization of electrospun polyvinyl alcohol nanofibrous scaffolds modified by blending with chitosan for neural tissue engineering. *International Journal of Nanomedicine*, *7*, 25.

Allafchian, A., Jalali, S. A. H., Mousavi, S. E., & Hosseini, S. S. (2020). Preparation of cell culture scaffolds using polycaprolactone/quince seed mucilage. *International Journal of Biological Macromolecules*, *155*, 1270-1276.

Camelo Caballero, L. R., Wilches-Torres, A., Cárdenas-Chaparro, A., Gómez Castaño, J. A., & Otálora, M. C. (2019). Preparation and physicochemical characterization of softgels cross-linked with cactus mucilage extracted from cladodes of *Opuntia Ficus-Indica*. *Molecules*, *24*, 2531.

Darwish, A. M., Khalifa, R. E., & El Sohaimy, S. A. (2018). Functional properties of chia seed mucilage supplemented in low fat yoghurt. *Alexandria Science Exchange Journal*, *39*, 450-459.

de Campo, C., Dos Santos, P. P., Costa, T. M. H., Paese, K., Guterres, S. S., de Oliveira Rios, A., & Flôres, S. H. (2017). Nanoencapsulation of chia seed oil with chia mucilage (*Salvia hispanica* L.) as wall material: Characterization and stability evaluation. *Food Chemistry*, *234*, 1-9.

Ellerbrock, R. H., Ahmed, M. A., & Gerke, H. H. (2019). Spectroscopic characterization of mucilage (chia seed) and polygalacturonic acid. *Journal of Plant Nutrition & Soil Science*, *182*, 888-895.

Fahami, A., & Fathi, M. (2018a). Development of cress seed mucilage/PVA nanofibers as a novel carrier for vitamin A delivery. *Food Hydrocolloids*, *81*, 31-38.

Fahami, A., & Fathi, M. (2018b). Fabrication and characterization of novel nanofibers from cress seed mucilage for food applications. *Journal of Applied Polymer Science*, *135*, 45811.

Fernandes, S. S., & de las Mercedes Salas-Mellado, M. (2017). Addition of chia seed mucilage for reduction of fat content in bread and cakes. *Food Chemistry*, *227*, 237-244.

Goh, K. K. T., Matia-Merino, L., Chiang, J. H., Quek, R., Soh, S. J. B., & Lentle, R. G. (2016). The physico-chemical properties of chia seed polysaccharide and its microgel dispersion rheology. *Carbohydrate Polymers*, *149*, 297-307.

Golkar, P., Kalani, S., Allafchian, A. R., Mohammadi, H., & Jalali, S. A. H. (2019). Fabrication and characterization of electrospun plantago major seed mucilage/PVA nanofibers. *Journal of Applied Polymer Science*, *136*, 47852.

Gu, S., Ren, J., & Vancso, G. (2005). Process optimization and empirical modeling for electrospun polyacrylonitrile (PAN) nanofiber precursor of carbon nanofibers. *European Polymer Journal*, *41*, 2559-2568.

Hadad, S., & Goli, S. A. H. (2018). Fabrication and characterization of electrospun nanofibers using flaxseed (*Linum usitatissimum*) mucilage. *International Journal of Biological Macromolecules*, *114*, 408-414.

Haghi, A., & Akbari, M. (2007). Trends in electrospinning of natural nanofibers. *Physica Status Solidi (a)*, *204*, 1830-1834.

Hamrang, A., & Howell, B. A. (Eds.). (2013). Foundations of high performance polymers: properties, performance and applications. CRC Press.

He, X., Deng, H., & Hwang, H. M. (2019). The current application of nanotechnology in food and agriculture. *Journal of Food & Drug Analysis*, *27*, 1-21.

Kayaci, F., Ertas, Y., & Uyar, T. (2013). Enhanced thermal stability of eugenol by cyclodextrin inclusion complex encapsulated in electrospun polymeric nanofibers. *Journal of Agricultural & Food Chemistry*, *61*, 8156-8165.

Kéri, O., Bárdos, P., Boyadjiev, S., Igricz, T., Nagy, Z. K., & Szilágyi, I. M. (2019). Thermal properties of electrospun

polyvinylpyrrolidone/titanium tetraisopropoxide composite nanofibers. *Journal of Thermal Analysis & Calorimetry, 137*, 1249-1254.

Kumar, T. S. M., Kumar, K. S., Rajini, N., Siengchin, S., Ayrilmis, N., & Rajulu, A. V. (2019). A comprehensive review of electrospun nanofibers: Food and packaging perspective. *Composites Part B: Engineering, 175*, 107074.

Kurd, F., Fathi, M., & Shekarchizadeh, H. (2017). Basil seed mucilage as a new source for electrospinning: Production and physicochemical characterization. *International Journal of Biological Macromolecules, 95*, 689-695.

Leidy, R., & Ximena, Q. C. M. (2019). Use of electrospinning technique to produce nanofibres for food industries: A perspective from regulations to characterisations. *Trends in Food Science & Technology, 85*, 92-106.

Liu, Y., Dong, L., Fan, J., Wang, R., & Yu, J. Y. (2011). Effect of applied voltage on diameter and morphology of ultrafine fibers in bubble electrospinning. *Journal of Applied Polymer Science, 120*, 592-598.

Londhe, P. V., Chavan, S. S., Pawar, A. M., & Shendokar, S. (2019). Optimization of parameters for diameter of nanofibers and FTIR, XRD characterization for synthesized biofunctionalized nanofibers (curcumin, gelatin and formic acid) using electrospinning process. *International Journal on Recent Technologies in Mechanical and Electrical Engineering, 6*, 10-23.

Menczel, J. D., & Prime, R. B. (Eds.). (2009). *Thermal analysis of polymers: fundamentals and applications*. John Wiley & Sons.

Motamedi, A. S., Mirzadeh, H., Hajiesmaeilbaigi, F., Bagheri-Khoulenjani, S., & Shokrgozar, M. (2017). Effect of electrospinning parameters on morphological properties of PVDF nanofibrous scaffolds. *Progress in Biomaterials, 6*, 113-123.

Noshad, M., Ghasemi, P., & Dehghani, S. (2019). Effect of Chia seed gum on physicochemical properties of powder production using foam-mat drying method. *Food Science & Technology, 16*, 343-351.

Okutan, N., Terzi, P., & Altay, F. (2014). Affecting parameters on electrospinning process and characterization of electrospun gelatin nanofibers. *Food Hydrocolloids, 39*, 19-26.

Sen, S., Bal, T., & Rajora, A. D. (2022). Green nanofiber mat from HLM–PVA–Pectin (*Hibiscus* leaves mucilage–polyvinyl alcohol–pectin) polymeric blend using electrospinning technique as a novel material in wound-healing process. *Applied Nanoscience, 12*(2), 237-250.

Şener, A. G., Altay, A. S., & Altay, F. (2011). Effect of voltage on morphology of electrospun nanofibers. In: 2011 7th International Conference on Electrical and Electronics Engineering (ELECO). Pp. I-324-I-328. IEEE.

Sousa, A. M., Souza, H. K., Uknalis, J., Liu, S.-C., Goncalves, M. P., & Liu, L. (2015). Electrospinning of agar/PVA aqueous solutions and its relation with rheological properties. *Carbohydrate Polymers, 115*, 348-355.

Urena-Saborio, H., Alfaro-Viquez, E., Esquivel-Alvarado, D., Madrigal-Carballo, S., & Gunasekaran, S. (2018). Electrospun plant mucilage nanofibers as biocompatible scaffolds for cell proliferation. *International Journal of Biological Macromolecules, 115*, 1218-1224.

Yang, J. M., Yang, J. H., Tsou, S. C., Ding, C. H., Hsu, C. C., Yang, K. C., Yang, C. C., Chen, K. S., Chen, S. W., & Wang, J. S. (2016). Cell proliferation on PVA/sodium alginate and PVA/poly (γ-glutamic acid) electrospun fiber. *Materials Science & Engineering: C, 66*, 170-177.

Zhang, C., Li, Y., Wang, P., & Zhang, H. (2020). Electrospinning of nanofibers: Potentials and perspectives for active food packaging. *Comprehensive Reviews in Food Science and Food Safety*, *19*(2), 479-502.